1566 *Inorg. Chem.* **2010**, *49*, 1566–1576
DOI: 10.1021/ic901888q

Inorganic Chemistry
Article

Density Functional Theory Study of the Electron Paramagnetic Resonance Parameters and the Magnetic Circular Dichroism Spectrum for Model Compounds of Dimethyl Sulfoxide Reductase

Elizabeth Hernandez-Marin, Michael Seth, and Tom Ziegler*

Department of Chemistry, University of Calgary, 2500 University Drive NW, Calgary, Alberta T2N 1N4, Canada

Received September 23, 2009

We report a density functional theory (DFT) study of electron paramagnetic resonance (EPR) parameters for complexes modeling the paramagnetic center Mo(V) of the molybdoenzyme dimethyl sulfoxide reductase. We pay special attention to the Mo−OH link to find the most likely geometry and orientation of the metal center in the enzyme and provide an analysis of the physical origin of the g-values in terms of magnetically induced orbital mixing. We also present a study of the magnetic circular dichroism (MCD) spectrum for a complex that models the Mo(V) center of the enzyme. The calculation of the MCD-parameters that give rise to the spectrum was performed using a newly implemented method based on time-dependent DFT. On the basis of the theoretical calculations, it was possible to give a full assignment of the bands of the MCD spectrum for the enzyme.

Introduction

The reductive deoxygenation of dimethyl sulfoxide to dimethyl sulfide is performed by bacteria from the genus *Rhodobacter*:[1,2]

$$(CH_3)_2SO + 2H^+ + 2e^- \rightarrow (CH_3)_2S + H_2O \qquad (1)$$

The enzyme responsible for this reaction is a mononuclear molybdoenzyme, which belongs to the DMSO reductase (DMSOR) family.[2−4] The two electrons in eq 1 are provided by the oxidation of the molybdenum center ($[Mo^{IV}] \rightarrow [Mo^{VI}]$). After the reduction of DMSO, for the molybdenum in the active site to return to the $[Mo^{IV}]$state, the enzyme should go through a $[Mo^{V}]$ oxidation state.[2]

Multiple spectroscopic studies on DMSOR from bacterial sources, such as X-ray crystallography, extended x-ray absorption fine structure (EXAFS), and electron paramagnetic resonance (EPR) have been carried out to determine its structure.[5−9] Moreover, a good number of spectroscopic studies on synthetic functional and structural analogues of the active site of the molybdoenzymes have been conducted.[10−12] As a result, there is a considerable body of information about the coordination geometry and spectroscopic properties of the molybdenum center in DMSOR. It has been established that the oxidized active site of DMSOR consists of the metal coordinated by two molybdopterin (metal binding pyranopterin ene-1,2-dithiolate) ligands, one oxo group, and one oxygen atom from the side chain of a serinyl residue.[6,13]

All EPR investigations indicate that for the enzyme in the $[Mo^{V}]$ state, there is one OH group coordinated to the metal center. However, the continuous-wave EPR studies did not allow for a detailed description of the $[Mo^{V}-OH]$ coordination structure. Recently, pulsed EPR methods were employed to elaborate on the details of the $[Mo^{V}-OH]$ mode.[9] We shall here supplement the experimental EPR investigations by density functional theory (DFT) calculations on the g-tensor

*To whom correspondence should be addressed. E-mail: ziegler@ucalgary.ca.

(1) Zinder, S. H.; Brock, T. D. *J. Gen. Microbiol.* **1978**, *335*, 655.
(2) Hille, R. *Chem. Rev.* **1996**, *96*, 2757.
(3) Satoh, T.; Kurihara, F. N. *J. Biochem.* **1987**, *102*, 191.
(4) McEwan, A. G.; Wetzstein, H. G.; Ferguson, S. J.; Jackson, J. B. *Biochim. Biophys. Acta* **1985**, *806*, 410.
(5) Li, H.; Temple, C.; Rajagopalan, K.; Schindelin, H. *J. Am. Chem. Soc.* **2000**, *122*, 7673.
(6) McAlpine, A.; McEwan, A.; Shaw, A.; Bailey, S. *J. Biol. Inorg. Chem.* **1997**, *2*, 690.
(7) George, G. N.; Hilton, J.; Temple, C.; Prince, R.; Rajagopalan, K. *J. Am. Chem. Soc.* **1999**, *121*, 1256.
(8) George, G. N.; Hilton, J.; Rajagopalan, K. V. *J. Am. Chem. Soc.* **1996**, *118*, 1113.
(9) Raitsimring, A.; Astashkin, A.; Feng, C.; Enemark, J.; Johnson Nelson, K.; Rajagopalan, K. *J. Biol. Inorg. Chem.* **2003**, *8*, 95.
(10) McNaughton, R.; Lim, B. S.; S., K.; Holm, R.; Kirk, M. *J. Chem. Soc.* **2008**, *130*, 4620.
(11) Nieter Burgmayer, S. J.; Kim, M.; Petit, M. L.; Rothkopf, A.; Kim, A.; BelHamdounia, S.; Hou, Y.; Somogyi, A.; Habel-Rodriguez, D.; Williams, A.; Kirk, M. *J. Inorg. Biochem.* **2007**, *101*, 1601.
(12) McNaughton, R.; Mondal, S.; V., N.; Basu, P.; Kirk, M. *Inorg. Chem.* **2005**, *44*, 8216.
(13) Tunney, J. M.; McMaster, J.; Garner, C. D. In *Comprehensive Coordination Chemistry II*; McCleverty, J. A., Meyer, T. J., Eds.; Elsevier: Amsterdam, 2003; Vol. *8*, p 459.

 Published on Web 01/21/2010

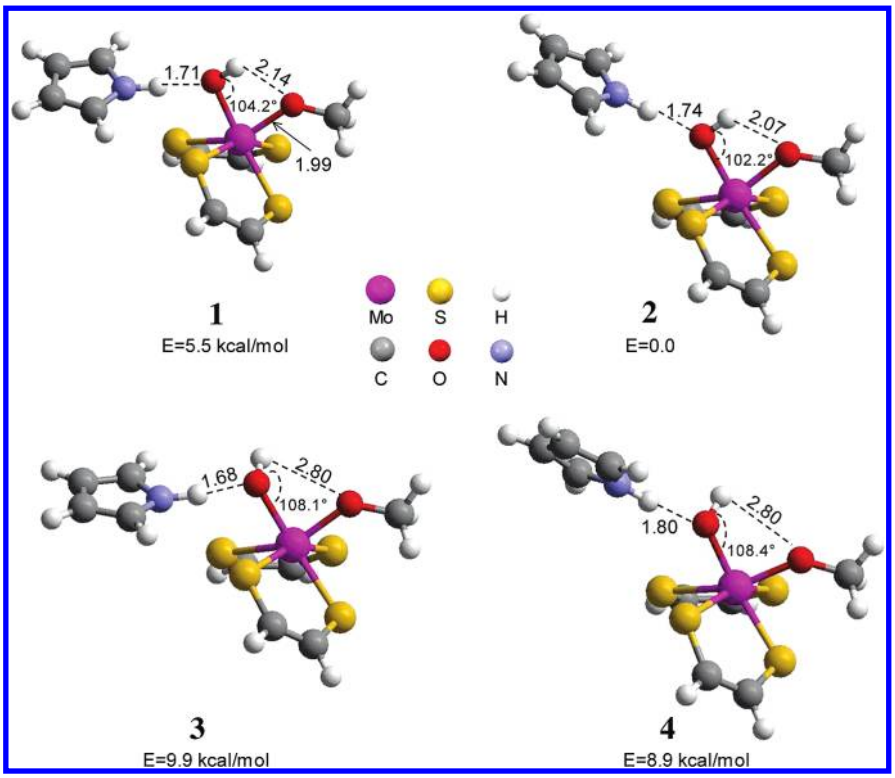

Figure 1. Optimized geometries for the model complexes **1**−**4**.

and the proton hyperfine coupling constant (HFC) of models for DMSOR in its [Mo^V] oxidation state to elucidate the [Mo^V−OH] coordination geometry. DFT calculations have had some success in the past reproducing the EPR parameters of transition metal complexes in general,[14−16] of several molybdenum complexes in particular,[17−21] and of molybdoenzymes such as sulfite oxidase.[22−24]

The electronic structure of DMSOR in its [Mo^V] oxidation state has also been studied by magnetic circular dichroism (MCD).[25,26] In an MCD experiment a sample is subjected to a constant magnetic field $\vec{B}$ and the difference in absorbance of right and left circularly polarized light (ΔA) propagating in the direction of $\vec{B}$ is measured. Of special interest has been the temperature dependent dent MCD represented by the so-called C-term.[27] We shall here carry out DFT calculations on the MCD spectrum of [Mo^V] model systems to help in the interpretation of the experimental spectrum for DMSOR. Such a study should help with the understanding of the electronic structure of DMSOR-Mo[V].

Computational Details and Methods

Computational Parameters. All calculations were based on DFT as implemented in the ADF program version 2006.01.[28] Use was made of the Becke−Perdew exchange-correlation functional (BP86)[29−31] and a standard triple-ζ STO basis with one set of polarization functions for all atoms. For the calculation of the g-tensors and MCD parameters, the 1s electrons of C, N, and O; the 1s2s2p electrons of S; and the 1s2s2p3s3p3d electrons of Mo were treated as frozen cores. The calculation of the ^{1}H hyperfine coupling did not use the frozen core option. The parameter for the precision of the numerical integration was set to 5.0.

Computational Model Systems for Mo[V]-DMSOR. The approximately trigonal prismatic models shown in Figure 1 were constructed based on the coordinates provided by the crystallographic structure of the oxidized Mo[VI] DMSO reductase from *Rhodobacter sphaeroides* (PDB code 1EU1).[5] From the crystal structure, the coordinates of the oxygen and carbon of the OMe group and of the sulfur and carbon atoms of the dithiolate groups were taken as those of Ser 147 and the pterin cofactors, respectively. The oxo ligand of the Mo[VI] system was substituted with a OH group, which is assumed to be present in the Mo[V]-DMSOR system. Additionally, the coordinates from the pyrrole group were taken from the corresponding group in the residue Trp 116. In the case of model **1**, the structure was fully optimized with the exception that the positions of the sulfurs from the dithiolate and the nitrogen from the pyrrole remained as in the X-ray structure of the oxidized system. For model **2**, the restrictions on the position of the nitrogen were

(14) Patchkovskii, S.; Ziegler, T. *J. Chem. Phys.* **1999**, *11*, 5730.
(15) Patchkovskii, S.; Ziegler, T. *J. Am. Chem. Soc.* **2000**, *122*, 3506.
(16) Saladino, A.; Larsen, S. *Catal. Today* **2005**, *105*, 122.
(17) Fritscher, J.; Hrobárik, P.; Kaupp, M. *J. Phys. Chem. B* **2007**, *111*, 4616.
(18) Fritscher, J.; Hrobárik, P.; Kaupp, M. *Inorg. Chem.* **2007**, *46*, 8146.
(19) Drew, S.; Young, C.; Hanson, G. *Inorg. Chem.* **2007**, *46*, 2388.
(20) Cosper, M. M.; Neese, F.; Astashkin, A. V.; Carducci, M. D.; Raitsimring, A. M.; H., E. J. *Inorg. Chem.* **2005**, *44*, 1290.
(21) Hadt, R. G.; Nemykin, V. N.; Olsen, J. G.; Basu, P. *Phys. Chem. Chem. Phys.* **2009**, *11*, 10377.
(22) Doonan, C. J.; Wilson, H. L.; Bennett, B.; Prince, R. C.; Rajagopalan, K. V.; George, G. N. *Inorg. Chem.* **2008**, *47*, 2033.
(23) Klein, E. L.; Astashkin, A. V.; Ganyushin, D.; Riplinger, C.; Johnson-Winters, K.; Neese, F.; H., E. J. *Inorg. Chem.* **2009**, *48*, 4743.
(24) Astashkin, A. V.; Klein, E. L.; Ganyushin, D.; Johnson-Winters, K.; Neese, F.; Kappler, U.; H., E. J. *Phys. Chem. Chem. Phys.* **2009**, *11*, 6733.
(25) Benson, N.; Farrar, J. A.; McEwan, A. G.; Thomson, A. J. *FEBS Lett.* **1992**, *307*, 169.
(26) Finnegan, M. G.; Hilton, J.; Rajagopalan, K. V.; Johnson, M. K. *Inorg. Chem.* **1993**, *32*, 2616.
(27) Kirk, M.; Peariso, K. *Curr. Opin. Chem. Biol.* **2003**, *7*, 220.
(28) Te Velde, G.; Bickelhaupt, F.; Baerends, E.; van Gisbergen, S.; Guerra, C.; Snijders, J.; Ziegler, T. *J. Comput. Chem.* **2001**, *22*, 931.
(29) Becke, A. *Phys. Rev. A: At., Mol., Opt. Phys.* **1998**, *38*, 3098.
(30) Perdew, J. *Phys. Rev. B* **1986**, *33*, 8822.
(31) Perdew, J. *Phys. Rev. B* **1986**, *34*, 7406.

lifted. With model **3**, the $H_{OH}-O_{OCH3}$ distance was constrained to 2.8 Å as proposed by Raitsimring et al. based on pulsed EPR experiments;[9] again, the positions of the sulfurs and nitrogen remained as in the X-ray structure of Mo [VI]-DMSOR. Model **4** was created by combining the six-coordinated molybdenum fragment from model **3** with the pyrrole group positioned as in model **2** and optimizing the structure while keeping the position of the sulfurs as in the other models and the $H_{OH}-O_{OCH3}$ distance constrained to 2.8 Å. The relative energies of the four models are given in Figure 1.

EPR Parameters. The calculation of the g-tensors were performed with the implementation due to Schreckenbach and Ziegler. This method is based on the use of gauge-including atomic orbitals (GIAO) and double perturbation theory.[32] Scalar relativistic effects were included within the quasi-relativistic framework[33] using relativistic frozen core potentials along with the first-order Pauli Hamiltonian. The computation of the ^{1}H hyperfine coupling constants was carried out with the implementation by van Lenthe et al.[34] within the relativistic zeroth order regular approximation (ZORA)[35] including the spin−orbit contribution.

The g-tensor, **g**, can be written as

$$\mathbf{g} = g_e\mathbf{1} + \Delta\mathbf{g} \tag{2}$$

where g_e is the g-value of the free electron, **1** is a 3 × 3 unit matrix, and $\Delta\mathbf{g}$ is the g-shift tensor.

The *st* component of the g-shift tensor has the following main contributions:[36]

$$\Delta g_{st} = \Delta g_{st}^{d} + \Delta g_{st}^{p} \tag{3}$$

where Δg_{st}^{d} and Δg_{st}^{p} are the diamagnetic and paramagnetic g-shift tensor terms, respectively. For the complexes considered here, the dominant contribution in eq 3 comes from the paramagnetic term; this term can be broken down further into contributions from the magnetic coupling between occupied and empty (virtual) orbitals (Δg_{st}^{ov}), and between occupied orbitals (Δg_{st}^{oo}):

$$\Delta g_{st}^{p} = \Delta g_{st}^{ov} + \Delta g_{st}^{oo} \tag{4}$$

Further, there are two main contributions to Δg_{st}^{ov}. One originates from the coupling between the lowest singly unoccupied molecular orbital (LSUMO), which we have chosen to be of β spin, and other occupied orbitals of β-spins. This contribution is usually positive for molybdenum d^1 complexes as discussed elsewhere.[14] The other contribution is negative, and it arises from the coupling between the highest singly occupied orbital (HSOMO) of α-spin and virtual orbitals of α-spin. In general, the paramagnetic shielding terms Δg_{st}^{ov} are obtained via the following expression:[36]

$$\Delta g_{st}^{ov} = 2\sum_{i}^{occ}\sum_{a}^{vir} u'^{ai}_{s}\langle\psi_i|\hat{h}^{t}_{SO}|\psi_a\rangle \tag{5}$$

where $\hat{h}^{t}_{SO}$ is the *t*-component of the spin−orbit operator, ψ_i and ψ_a represent occupied and virtual orbitals, respectively, and the term u'^{s}_{ai} is given by

$$u'^{ai}_{s} \propto \frac{\langle\psi_i|\hat{L}^{s}|\psi_a\rangle}{\varepsilon_i - \varepsilon_a} \tag{6}$$

where $\hat{L}^{s}$ is the *s*-component of the one electron-angular momentum operator, and ε_i and ε_a are the energies of occupied orbital ψ_i and virtual orbital ψ_a, respectively.

It is known that GGA functionals such as BP86 tend to overestimate the covalency of metal−ligand bonds.[37] This overestimation is responsible for the high values of the g-tensor obtained at the BP86 level.[19] Several studies on molybdenum complexes indicate that although the overestimation on the g-terms is around 0.5−2% from the experimental values, the experimental trends are well reproduced.[17−19]

The nuclear hyperfine interaction is the interaction of an unpaired electron and a magnetic nucleus ν. The Hamiltonian that describes this interaction is[38]

$$\hat{H} = \hat{I}\cdot\mathbf{A}\cdot\hat{S} \tag{7}$$

where **A** is the hyperfine coupling tensor, and $\hat{S}$ and $\hat{I}$ are the spin operators of the electron and nucleus, respectively. The components of the **A** tensor for nucleus ν in eq 7 can be calculated as[34]

$$A_{kl} = \frac{g_e g_\nu}{4Mc^2}\int\left[3\frac{r_{k\nu}r_{l\nu}}{r_\nu^5} - \frac{\delta_{kl}}{r_\nu^3} + \frac{8\pi}{3}\delta(r_\nu)\delta_{kl}\right](\rho_\alpha - \rho_\beta)\,\mathrm{d}^3r_\nu \tag{8}$$

where g_ν is the g-value of the nucleus ν, and M the proton mass in units of the electron mass. The position of the electron relative to the position of the nucleus is represented by r_ν, and ρ_α and ρ_β are the densities of electrons with α- and β-spin, respectively. The first two terms of the integral describe the dipolar hyperfine interaction that gives rise to any observed anisotropy, and the third one represents the Fermi contact term that is responsible for the isotropic hyperfine interaction.

MCD Spectrum. In MCD spectroscopy one subjects a sample to a constant magnetic field ($\vec{B}$) and measures the difference in absorbance between left and right circularly polarized light (ΔA) traveling in the direction of $\vec{B}$. The MCD dispersion can be expressed as a function linear in the applied magnetic field strength B:[39]

$$\frac{\Delta A}{E} = \gamma B\left[A\left(-\frac{\partial f(E)}{\partial E}\right) + \left(B + \frac{C}{kT}\right)f(E)\right] \tag{9}$$

where γ is a collection of constants, k is the Boltzmann constant, and T, the temperature. Further, $f(E)$ is a band shape function and E is the energy of the incident radiation. The constants A, B, and C are characteristic parameters specific to a given molecule and to a particular transition. It is customary to refer to the contributions in eq 9 containing A, B, and C as A-, B-, and C-terms, respectively. At low temperatures, the temperature dependent C-terms seen for paramagnetic systems, dominate over the A- or B- terms.[27]

The simulated MCD spectrum was obtained by the use of an approach developed by Seth et al.[40] that calculates the C parameter by including spin−orbit perturbations. This method has been implemented into the ADF program, and it makes use of time-dependent DFT (TDDFT)[41] to describe the electronic excitations[42] and the zero-order regular approximation (ZORA) formalism to include relativistic effects.[35] The C_J parameter induced by the perturbation of the transition dipole for the

(32) Schreckenbach, G.; Ziegler, T. *J. Phys. Chem. A* **1997**, *101*, 3388.
(33) Ziegler, T.; Tschinke, V.; Baerends, E.; Snijders, J.; Ravenek, W. *J. Phys. Chem.* **1989**, *93*, 3050.
(34) van Lenthe, E.; van der Avoird, A.; Wormer, P. *J. Chem. Phys.* **1998**, *108*, 4783.
(35) van Lenthe, E.; Baerends, J.; Snijders, J. *J. Chem. Phys.* **1993**, *99*, 4597.
(36) Schreckenbach, G. *Relativity and Magnetic Properties. A Density Functional Study*. Ph.D. Thesis, University of Calgary, Calgary, Canada, **1996**.
(37) Swann, J.; Westmoreland, D. *Inorg. Chem.* **1997**, *36*, 5348.
(38) Wertz, J.; Bolton, J. *Electron Spin Resonance*; Chapman and Hall: New York, 1996.
(39) Stephens, P. *Annu. Rev. Phys. Chem.* **1974**, *25*, 201.
(40) Seth, M.; Ziegler, T.; Autschbach, J. *J. Chem. Phys.* **2008**, *129*, 104105.
(41) Casida, M. In *Advances in Density Functional Methods*; Chong, D. P., Ed.; World Scientific: Singapore, 1995; Vol. *1*, p 155.
(42) Wang, F.; Ziegler, T. *Mol. Phys.* **2004**, *102*, 2585.

excitation $A \rightarrow J$ in the γ direction by spin−orbit coupling can be written as[40]

$$C_J \propto \sum_{\alpha\beta\gamma} \varepsilon_{\alpha\beta\gamma} \langle A|M^{\alpha}|J\rangle^{(1)\gamma} \langle J|M^{\beta}|A\rangle^{(0)} \tag{10}$$

where $\varepsilon_{\alpha\beta\gamma}$ is the Levi−Civita symbol (if $\alpha\beta\gamma$ is a cyclic permutation of xyz, $\varepsilon_{\alpha\beta\gamma} = 1$, otherwise is $= -1$ or $= 0$ when $\alpha = \beta$, $\alpha = \gamma$ or $\beta = \gamma$), M^{α} and M^{β} correspond to the Cartesian components for the electric dipole moment operator, A refers to the ground state, J to a given excited state, and the superscripts (1) and (0) indicate the first order spin−orbit perturbed and unperturbed integrals, respectively.

It should be noted that response theory is employed for the evaluation of the C-parameters, and a detailed description of such calculations can be found elsewhere.[40] However, the term $\langle A|M^{\alpha}|J\rangle^{(1)\gamma}$ of eq 10 can be written formally as a sum-over-states expression:

$$\langle A|M^{\alpha}|J\rangle^{(1)\gamma} = \sum_{K' \neq A} \langle K'|M^{\alpha}|J\rangle^{(0)} \frac{\langle K'|H_{SO}^{\gamma}|A\rangle^{(0)}}{E_{K'} - E_A} + \sum_{K \neq J} \langle A|M^{\alpha}|K\rangle^{(0)} \frac{\langle J|H_{SO}^{\gamma}|K\rangle^{(0)}}{E_K - E_J} \tag{11}$$

where H_{SO} is the spin−orbit operator.

For qualitative analysis purposes, inspection of the eqs 10 and 11 allows one to write a simplified expression for the C-parameter as

$$C_J = C_J^G + C_J^E \tag{12}$$

where C_J^G represents the contribution due to the mixing of the ground state with excited states via spin orbit coupling and C_J^E represents the contribution due to the mixing of excited state J with other excited states.

We thus have

$$C_J^G = \sum_{\alpha\beta\gamma} \varepsilon_{\alpha\beta\gamma} \sum_{K' \neq A} \langle K'|M^{\alpha}|J\rangle^{(0)} \langle J|M^{\beta}|A\rangle^{(0)} \frac{\langle K'|H_{SO}^{\gamma}|A\rangle^{(0)}}{E_{K'} - E_A} \tag{13}$$

and

$$C_J^E = \sum_{\alpha\beta\gamma} \varepsilon_{\alpha\beta\gamma} \sum_{K \neq J} \langle A|M^{\alpha}|K\rangle^{(0)} \langle J|M^{\beta}|A\rangle^{(0)} \frac{\langle J|H_{SO}^{\gamma}|K\rangle^{(0)}}{E_K - E_J} \tag{14}$$

We shall later, on the basis of our calculations, discuss the relative importance of C_J^E and C_J^G for the MCD spectrum of our model system. It is interesting to point out that the paramagnetic contribution Δg_{st}^p to the g-shift tensor Δg of eq 3 can also be written in terms of a sum-over-states expression:[43]

$$\Delta g_{st}^p \propto \sum_{K' \neq A} \langle A|L^s|K'\rangle \frac{\langle K'|H_{SO}^t|A\rangle}{E_{K'} - E_A} \tag{15}$$

where L^s is a component of the magnetic moment operator and H_{SO}^t, a component of the spin−orbit operator. We note that the sum-over-states expression in eq 15 is in terms of many-electron wave functions and operators, whereas the response expressions of eqs 5−6 are in terms of one-electron orbitals and operators.

(43) Kaupp, M.; Buhl, M.; Malkin, V. *Calculation of NMR and EPR parameters. Theory and Applications*; Wiley-VCH: Germany, 2004; pp 526−534.

Table 1. Experimental and Calculated EPR Parameters[a] for Model Systems of Mo[V]-DMSOR

	g_1	g_2	g_3	^{1}H A^{iso}	A_1	A_2	A_3
avg. exp. DMSOR[b]	1.9923	1.9821	1.9664	32.81	30.45	29.19	38.78
model **1**	2.0140	1.9911	1.9849	29.87	26.8	24.8	38.0
model **2**	2.0146	1.9908	1.9839	35.6	32.7	30.2	43.9
model **3**	2.0031	1.9875	1.9776	4.09	0.4	−2.1	13.9
model **4**	1.9993	1.9843	1.9702	24.56	21.3	19.2	33.2

[a] Hyperfine coupling constants are in MHz. [b] We present the average value obtained from EPR parameters reported in refs 7 and 44.

It is thus clear, from a comparison of eqs 13 and 15, that both Δg^p and C_J^G depend in a similar way on the coupling of the ground state (A) and excited states (K') through the spin−orbit coupling H_{SO}. We shall discuss later to what degree this similarity gives rise to correlations between Δg and the C-parameters.

Results and Discussion

A direct computational determination of the coordination geometry around the molybdenum center in Mo[V]-DMSOR is not possible without including a sizable part of the protein environment. Modeling on such a scale is costly and has not been undertaken here. We shall instead calculate EPR parameters for various simple models of Mo^V−DMSOR with different coordination geometries and orientations of the Mo−OH link. We hope from such a comparison to explore which model affords the best fit to the observed EPR parameters for the enzyme. We shall further provide a detailed discussion of the dominant contributions to Δg^{ov} from interactions between occupied and virtual orbitals due to spin−orbit couplings (eq 5). This will also prepare us for a discussion of the MCD spectrum for Mo[V]-DMSOR where such couplings are important as well.

EPR Parameters. The EPR investigations of DMSOR of *R. capsulatus* have shown that the conditions of the sample preparation, for example whether it was prepared by reduction or oxidation, slightly influence the value of the EPR parameters. The experimental g- and A-values range were found to be as follows: $g_1 = 1.9937-1.9904$, $g_2 = 1.9830-1.9818$, and $g_3 = 1.9686-1.9651$; $A_1 = 40.63-43.16$ MHz, $A_2 = 29.43-35.03$ MHz, and $A_3 = 32.22-32.78$ MHz.[44] For the case of experiments on Mo[V]-DMSOR of *R. sphaeroides*, the dependence on the sample preparation was also reported: $g_1 = 1.9924-1.9916$, $g_2 = 1.9813-1.9815$, and $g_3 = 1.9645-1.9650$; $A_1 = 33.3-38.0$ MHz, $A_2 = 24.5-27.8$ MHz, and $A_3 = 26.1-30.7$ MHz.[7] The average of the experimental g-tensor values is presented in Table 1 along with the corresponding average of the experimental ^{1}H HFC constants. It is clear that all the experimental g-values appear below the free electron value of $g_e = 2.0023$. We shall now compare the calculated EPR parameters from various models with the experimental data to determine the most likely [Mo^V−OH] coordination geometry. The orientation of the three principal axes corresponding to g_1, g_2, and g_3, as well as to the principal components of the A-tensor of the ^{1}H from the hydroxide ligand, are shown in Figure 2. It can be seen that the axis systems of the g- and A-tensor do not coincide.

(44) Bennet, B.; Benson, N.; McEwan, A.; Bray, R. *Eur. J. Biochem.* **1994**, *225*, 321.

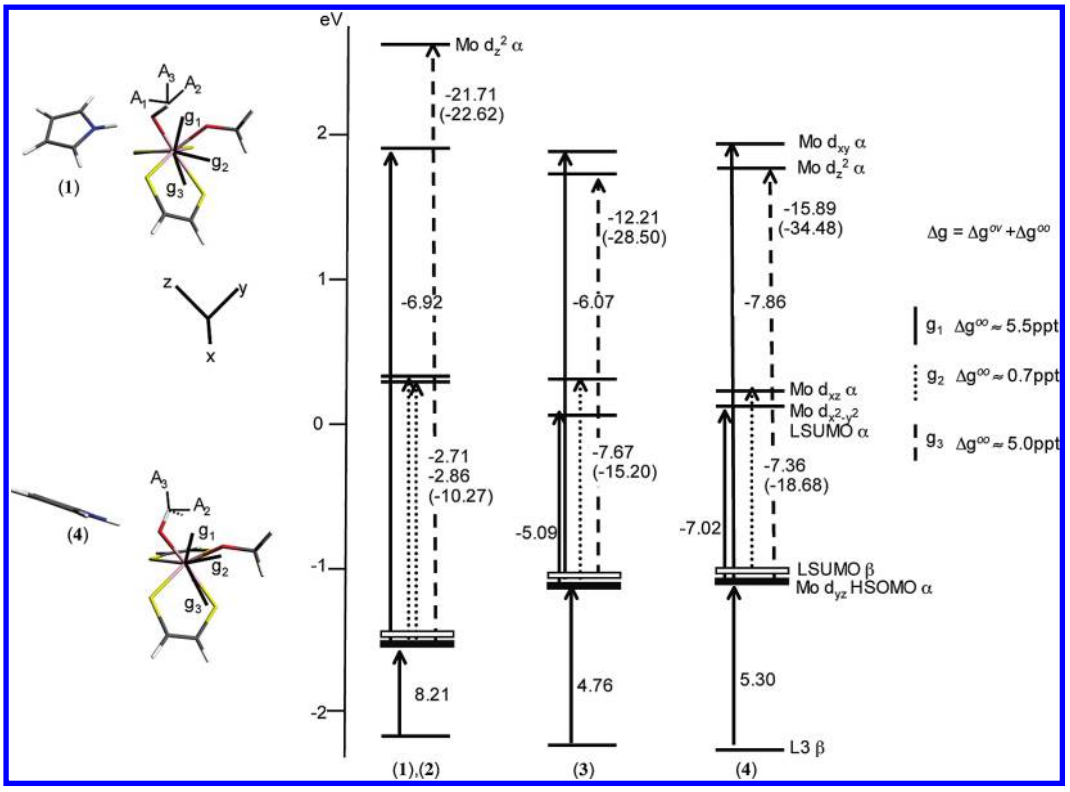

Figure 2. Schematic description of the main contributions (Δg^{ov},Δg^{oo}) to the principal g-values, g_1, g_2 and g_3 for each discussed model. The most important contributions to the total value of Δg_i^{ov} are shown, broken down into those from the magnetic coupling between the LSUMO of β-spin and occupied β orbitals as well as the HSOMO of α-spin and virtual α orbitals. The numbers is parentheses represent the total value of the respective Δg_i^{ov} contribution as listed in Table 2.

Table 2. Main Contributions[a] to the Principal Components of Δg for Model Systems of Mo[V]- DMSOR

	g_1		g_2		g_3	
model	Δg^{ov}	Δg^{oo}	Δg^{ov}	Δg^{oo}	Δg^{ov}	Δg^{oo}
1	4.26	6.46	−10.27	0.69	−22.62	5.53
2	4.74	6.45	−10.46	0.71	−23.52	5.39
3	−4.94	5.34	−15.20	0.51	−28.50	4.67
4	−9.14	4.40	−18.68	0.76	−34.48	4.25

[a] Contributions in parts per thousand.

We start our discussion of the calculated EPR parameters by considering model **1** in Figure 1. Here we froze the positions of the sulfurs from the thiolates as well as the nitrogen of the pyrrole to those of the experimental X-ray structure of Mo[VI]-DMSOR while optimizing all other degrees of freedom. Table 1 indicates that the three principal ^{1}H HFC values of model **1** are in good agreement with the experimental estimates. Nevertheless, opposite to the experimental results, the g_1 component of the g-tensor was calculated to be larger than g_e. Table 2 shows that the contribution due to the coupling between occupied orbitals (Δg_1^{oo}) and from the coupling between occupied and virtual orbitals (Δg_1^{ov}) are both positive. Thus, by applying eq 4, the paramagnetic contribution is positive, rendering the g_1 component larger than that of the free electron value. The two remaining components, g_2 and g_3, are in better agreement with the experimental results. In both cases, the g-values are smaller than g_e because the negative contribution to the paramagnetic g-shift represented by Δg^{ov} is larger, in absolute terms, than the contribution of the coupling between occupied orbitals (Table 2). Figure 2 displays the coupling orbitals that give rise to the Δg_i^{ov} term. All the models represent a d^1 coordination complex, therefore they have one unpaired electron. This unpaired electron of α-spin sits in the highest singly occupied molecular orbital (HSOMO α), in this case, an orbital that we called Mo d_{yz} as shown in Figure 3. Since we have an unpaired α electron, the corresponding empty orbital of β-spin represents the LSUMO β. It should be noted that the total Δg_i^{ov} term is made up from the coupling between the HSOMO α (Mo d_{yz} α) with virtual orbitals of α-spin, and the coupling of the LSUMO β (Mo d_{yz} β) with occupied orbitals of β-spin.

In the case of model **1**, Figure 2 shows that the value of Δg_1^{ov} is mostly due to a contribution from the coupling between the Mo d_{yz} and the Mo d_{xy} α orbitals, whereas one important positive contribution of 8 ppt (parts per thousand) is due to the coupling between the β-spin L3 and the Mo d_{yz} orbitals. The L3 orbital is displayed in Figure 4. The coupling between the α-spin orbitals Mo d_{yz} and the orbital Mo $d_{x^2-y^2}$, where the MO that we call Mo $d_{x^2-y^2}$ has also some contribution from a d_{xz} orbital, plus the coupling between α Mo d_{yz} and Mo d_{xz} (−2.71 and −2.86 ppt, respectively) constitute the main source for the negative Δg_2^{ov} contribution (Table 2), while the coupling between the Mo d_{yz} and Mo d_{z^2} α orbitals yields almost all of the negative Δg_3^{ov} component. In quantitative terms, we see that the negative values for Δg_2^{ov} and Δg_3^{ov} offset the positive contributions to g_2 and g_3 from Δg_2^{oo} and Δg_3^{oo}, see Figure 2 and Table 2. Consequently,

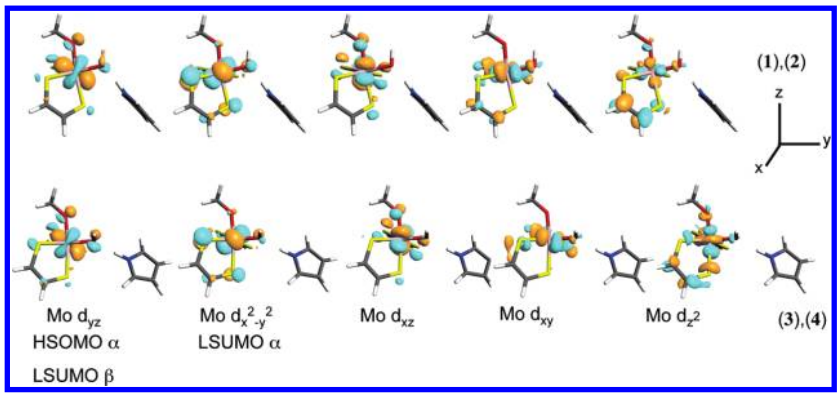

Figure 3. Plots of metal based orbitals in the four model complexes. The orbital named Mo $d_{x^2-y^2}$ contains a considerable contribution from the d_{xz} orbital.

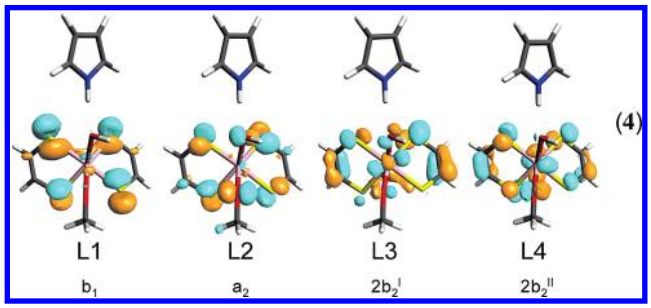

Figure 4. Plots of ligand based orbitals. The labels a_2, b_1, and $2b_2$ refer to the molecular fragment in Figure 6.

the g_2 and g_3 components are calculated to be smaller than g_e as are the experimental values for Mo^V−DMSOR. In contrast, for the g_1 component, the Δg_1^{ov} and Δg_1^{oo} are both positive, thus rendering $g_1 > g_e$.

Model **2** is a modification of **1** in that the positions of the sulfurs remained frozen but the pyrrole group was allowed to move freely without fixing the nitrogen. The pyrrole group rearranged as depicted in Figure 1. However, Table 1 indicates that the g-values remained unaffected with respect to model **1**. In fact, the g-tensor has the same physical origin as in model **1**, as shown in Table 2. The total value of $\Delta g_1^{ov} = 4.74$ ppt comes mostly from the coupling between the Mo d_{yz} and Mo d_{xy} α-spin orbitals (−8.7 ppt) and the coupling between the L5 and Mo d_{yz} β orbitals (+9.3 ppt). As in model **1**, the Δg_1^{ov} and Δg_1^{oo} terms yield an overall positive Δg_1 that gives a g_1 component larger than the free-electron value. Likewise, Δg_2^{ov} arises mainly from the coupling between the Mo d_{yz} and Mo $d_{x^2-y^2}$ α orbitals (−3.7) plus the α Mo d_{yz}− d_{xz} coupling (−1.5 ppt), and the Δg_3^{ov} is mostly due to the α Mo d_{yz}−Mo d_{z^2} coupling. The rearrangement of the pyrrole group has a significant impact on the isotropic HFC value, which increases from 26.8 MHz in model **1** to 32.7 MHz in model **2**. In terms of energy, model **2** is 5.5 kcal/mol more stable than model **1**.

Model **3** in Figure 1 differs from **1** in that we have introduced an additional constraint: the H_{OH}−O_{OCH3} length is frozen at 2.8 Å in accordance with the estimated distance obtained by Raitsimring et al.[9] based on continuous-wave EPR experiments. The positions of the sulfurs and nitrogen were frozen as in model **1**. The rest of the degrees of freedom were optimized. The energy of model **3** is 4.4 kcal/mol above model **1** because of the H_{OH}−O_{OCH3} constraint. In this model we see that the calculated EPR parameters differ significantly from the two other models that have been discussed so far. On the one hand, Table 1 shows that **3** produces, for the OH proton, A-components that are extremely small with respect to the experimental values by decreasing the valence spin density of the s orbital on the H atom from the OH ligand. On the other hand, the agreement with the experimental g-values is improved. From Table 2, we see that the contributions to the paramagnetic g-shift due to the coupling between occupied orbitals is somehow similar for all models. Although the Δg_1^{ov} contribution is now negative, the g_1 component of model **3** is still slightly larger than g_e because the negative Δg^{ov} term is smaller (−4.94 ppt, Table 2), in absolute value, than the Δg^{oo} term (5.3 ppt). It is possible to explain the difference between the main contributions to Δg_1^{ov} due to the coupling of β orbitals in models **1** and **3** by means of eqs 5 and 6. First, the molecular β-spin orbitals Mo d_{yz} and L3 displayed in Figures 3 and 4 are essentially similar, so we assume that the matrix element $\langle\psi_i|\hat{L}|\psi_a\rangle$ should be similar in both cases. However, we notice in Figure 2 that the orbital energy levels are quite different. For example, the energy difference $(\varepsilon_{L3} - \varepsilon_{Mod_{yz}})$ is larger for **3** than for **1**. Because the Δg_{st}^{ov} term is inversely proportional to the energy difference, we see that the contribution to Δg_1^{ov} due to the β L3 − Mo d_{yz} coupling is 8.21 ppt for **1** and 4.76 ppt for **3**, see Figure 2. On the other hand, when the couplings between α-orbitals are examined, it is found that for model **1** the principal contribution to the Δg_1^{ov} is due to the Mo d_{yz}− Mo d_{xy} coupling. But in the case of model **3** there now appears an additional contribution of similar value from the coupling between the Mo d_{yz} and Mo d_{x^2y2} orbitals. Then for model **3**, these two contributions of negative value, combined with the positive contribution from the coupling of the β-orbitals, give an overall negative value of $\Delta g_1^{ov} = -4.94$ ppt. In the case of model **1**, the negative contributions from the α-couplings turn out to be outweighed by the positive contributions for a total value of $\Delta g_1^{ov} = 4.26$ ppt.

The last model to be fully discussed is **4**. This structure was constructed with the combination of the six-coordinated molybdenum fragment from model **3** with pyrrole group positioned as in model **2**. The optimization constrained the H_{OH}−O_{OCH3} distance to 2.8 Å and froze the position of the sulfurs as in the X-ray structure of Mo[VI]-DMSOR. Model **4** was found to be 8.9 kcal/mol above model **2** and 1 kcal/mol below model **3**.To ensure that the

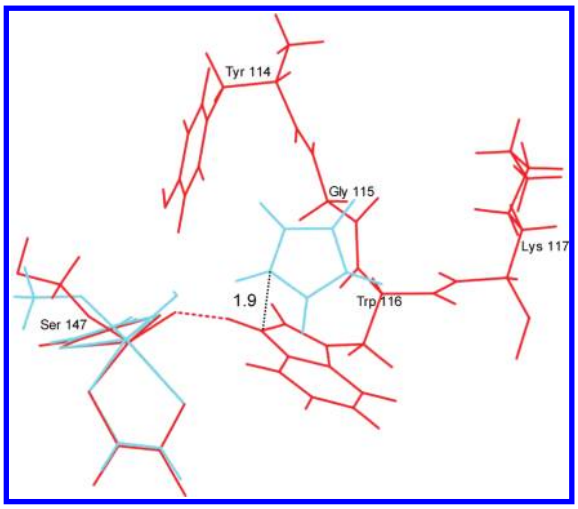

Figure 5. Superposition of a fragment from the crystal structure of DMSOR in red and model (**4**) in light blue.

new orientation of the pyrrole group does not interfere with other residues in the protein, model **4** was superimposed with a fragment of DMSOR that comprises the active site and residues 114 to 116. Figure 5 shows that the pyrrole (from the side chain of the tryptophan residue) can, in principle, adopt an orientation as suggested by model **4**. Moreover, Table 1 show that this last model improved notably the agreement with all EPR parameters, especially with the hyperfine coupling and the g_1 component. The g_2 and g_3 components remained nearly identical to the values of model **3**. With respect to the component g_1, the two couplings between the α Mo d_{yz} and Mo d_{xy} and between α Mo d_{yz} and Mo $d_{x^2-y^2}$ represent the main contributions to the total value of $\Delta g_1^{ov} = -9.14$ ppt. From Table 2, we see that $\Delta g_1^{oo} = 4.40$ ppt and consequently, the overall g_1 component is smaller than g_e. Such result is in agreement with the experimental results. Although the molecular orbitals of **3** and **4** are qualitatively similar, their respective Δg_1^{ov} is slightly different. If we consider that the energy difference between the orbitals is very similar for the two models, the subtle differences in their respective compositions may give rise to the quantitative differences on the overall value of Δg_1^{ov}. Those differences would affect the value of the corresponding $\langle \psi_i | \hat{L} | \psi_a \rangle$ matrix elements from eq 6. For example, the sum of the two α-couplings previously discussed and shown in Figure 2 yield a combined contribution of −14.88 ppt to the overall value of Δg_1^{ov} for model **4**. In the case of **3**, the same couplings contribute with −11.66 ppt. Likewise, the discussed β-couplings are 4.76 and 5.30 ppt for **3** and **4**, respectively (Figure 2).

An additional structure (not shown) keeping only one constraint, the $H_{OH}-O_{OCH3}$ distance, was optimized. This structure favored a more stable, with respect to the trigonal prismatic geometry, distorted octahedral geometry and gave an isotropic proton HFC of 46.8 MHz and a g-tensor with principal values $g_{\|} = 1.9702$ and $g_{\perp} = 1.9945$. Since the experimental g-tensor shows three distinct g-values, it is clear that the actual enzyme keeps the trigonal prismatic geometry all along the catalytic cycle. From our discussion, we conclude that the calculated A- and g-tensor afford the best combined fit for model **4**.

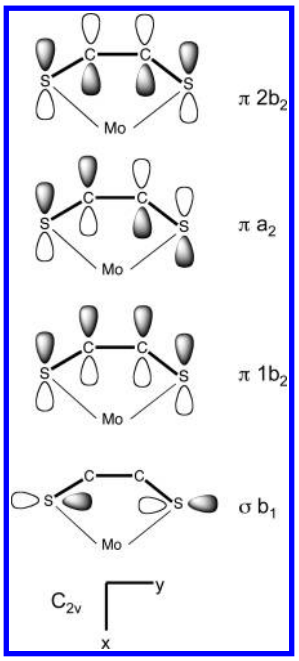

Figure 6. Some of the linear combinations of ligand p-orbitals used to assign the MCD-bands from the experimental spectra. Adapted from refs 25 and 26.

MCD Spectrum. Since the g-tensor and the *C*-parameters are somehow related (see eqs 11 and 15) we decided to also conduct calculations of MCD-parameters. At the beginning of the Results and Discussion section we mentioned the reason (computational cost) behind the use of a relatively small (compared with the enzyme) model to calculate the EPR parameters. We have for the same reason used a small model in the calculation of the MCD parameters. Moreover, in the model systems previously discussed in this study, it was found that the pyrrole group does not play a very significant role for the physical origin of the g-tensor. Consequently, the simulation of the MCD spectrum was conducted on a model based on **4** that does not include the pyrrole group. On the basis of that model, we shall provide a detailed discussion of the dominant contributions to the *C*-parameters that give rise to the MCD spectrum of our model and hopefully also for the enzyme. A point of clarification on the terminology should be made: throughout the text, "*C*-parameter" refers to the calculated numerical value for a given excitation, while "C-term" is used to describe the different bands that make up the MCD spectrum.

Before starting with the assignment and interpretation of the simulated MCD spectrum, we will turn to the discussion of the calculated absorption spectrum and the description of the most important excitations in terms of contributions from one electron transitions as calculated by means of TDDFT.

The simulated absorption spectrum shown in Figure 8 consists of 5 bands located around 10500 (B_1), 16000 (B_2), 19000 (B_3), 22500 (B_4), and 25000 (B_5) cm^{-1}. According to Figure 8, the B_1 band consists of excitations 1,2, 3, and 4; while the B_2 band is composed of excitations 5, 6, and 7. The band B_3 is mainly due to the excitations 8 and 9, and some of the components of band B_4 are excitations 10, 11, 12, and 13. Finally, B_5 includes excitations 14, 15, and 16. The composition of all the mentioned excitations (1−16)

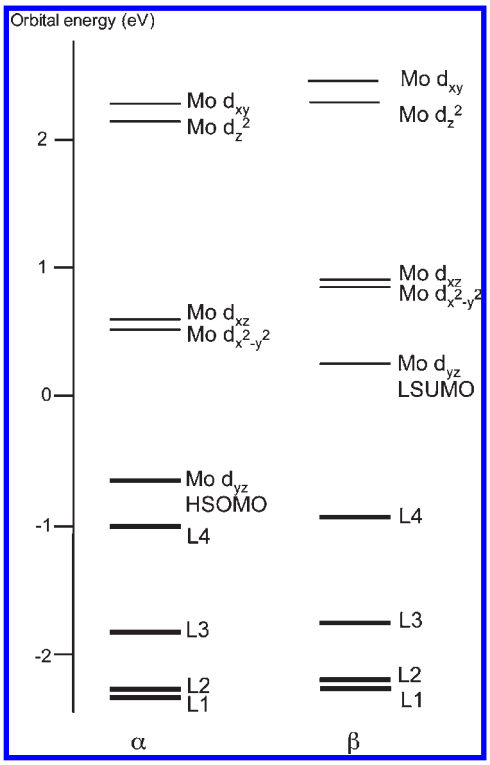

Figure 7. Orbital energy diagram and plot of the key occupied and virtual orbitals that contribute to the discussed one-electron excitations. The d-orbitals are shown in Figure 3, and the ligand orbitals labeled L1-L4 are shown in Figure 4.

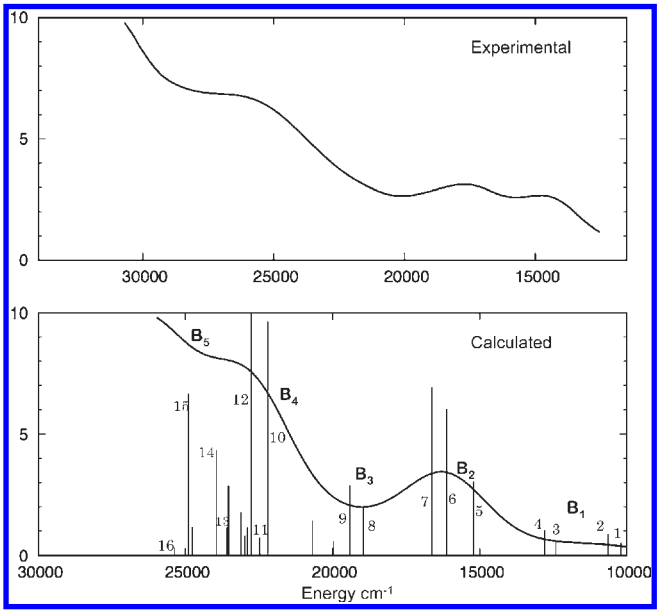

Figure 8. Simulated absorption spectrum. The bars underneath the five labeled bands indicate the absorbance of each transition contributing to the band.

is listed in Table 3. Additionally, the key metal-based orbitals and ligand-based orbitals involved in the one-electron transitions are presented in Figures 3 and 4, respectively. Their corresponding orbital level diagram appears in Figure 7. Table 3 shows that the excitations forming the weak band B_1 are mostly made up of one-electron transitions between orbitals of α-spin. Excitations 1 and 2 are d-d transitions dominated by the

Table 3. Calculated Excitation Energies, Oscillator Strength (*f*), and Assignment of Selected One-Electron Excitations for a Model System (**4′**)[b] of Mo[V]-DMSOR

band	excitation	excitation energy[a]	composition[c]	%	*f*
B_1	1	10200	α Mo d_{yz} → Mo $d_{x^2-y^2}$	86.7	0.0008
	2	10630	α Mo d_{yz} → Mo d_{xz}	90.0	0.0013
	3	12420	α L4 → Mo $d_{x^2-y^2}$	70.3	0.0008
	4	12800	α L4 → Mo d_{xz}	68.4	0.0016
B_2	5	15210	β L4 → Mo $d_{x^2-y^2}$	72.0	0.0046
	6	16120	β L4 → Mo d_{xz}	46.6	0.0091
			β L3 → Mo d_{yz}	31.4	
	7	16630	β L3 → Mo d_{yz}	64.5	0.0104
B_3	8	18950	α L3 → Mo $d_{x^2-y^2}$	48.6	0.0029
	9	19410	α L3 → Mo d_{xz}	46.8	0.0044
B_4	10	22200	β L3 → Mo $d_{x^2-y^2}$	48.5	0.0146
	11	22460	α L2 → Mo $d_{x^2-y^2}$	55.7	0.0011
	12	22760	α Mo d_{yz} → Mo d_{z^2}	54.1	0.0151
	13	23580	α Mo d_{yz} → Mo d_{xy}	67.9	0.0018
B_5	14	23950	α L3 → Mo d_{xz}	23.1	0.0066
			α L1 → Mo d_{yz}	14.2	
	15	24880	β L2 → Mo $d_{x^2-y^2}$	30.2	0.0100
			β L4 → Mo d_{yz}	15.6	
	16	25360	β L1 → Mo $d_{x^2-y^2}$	49.1	0.0005
			β L2 → Mo $d_{x^2-y^2}$	13.9	

[a] Energies in cm^{-1} and (nm). [b] Model system **4′** is identical to **4** of Figure 1 without the pyrrole ring. [c] The orbitals are shown in Figures 3 and 7.

excitation of the electron on the α-SOMO orbital (Mo d_{yz}) to the metal-based orbital Mo $d_{x^2-y^2}$ and Mo d_{xz}, respectively. Meanwhile, excitations 3 and 4 are mainly due to the transition of an electron from the ligand-based orbital L4 to a metal-based orbital Mo $d_{x^2-y^2}$ and Mo d_{xz}, respectively. Figure 4 shows that the L4 orbital keeps some resemblance to the $2b_2(\pi)$ combination of the simple ligand fragment in Figure 6. Next, the excitations that form the band B_2 can be described as transitions involving the transition of a β-spin electron from orbital L4 to Mo $d_{x^2-y^2}$ (excitation 5), L4 to Mo d_{xz} (excitation 6), and L3 to Mo d_{yz} (excitation 7). In this case, the orbital L3 is also similar to the $2b_2(\pi)$ combination in Figure 6. Following, the band B_3 consists mainly of excitations 8 and 9. The former is represented by an L3 → Mo $d_{x^2-y^2}$ transition, and the latter by an L3 → Mo d_{xz} transition, both involving mostly α-electrons. The band B_4 is made up of multiple excitations of which the most intense ones are 10 and 12. Excitation 10 is made from the β L3 → Mo $d_{x^2-y^2}$ transition. The d-d transition α Mo d_{yz} → Mo d_{z^2} is represented by excitation 12. Although excitations 11 (β L2 → Mo $d_{x^2-y^2}$) and 13 (d-d transition Mo d_{yz} → Mo d_{xy}) are weak, they are included for a complete discussion on the origin of the MCD spectra. Finally, 14 and 15 constitute the most intense excitations under the B_5 band. According to Table 3, excitation 14 is composed by a mixture of α L3 → Mo d_{xz} and α L1 → Mo d_{yz} transitions. On the other hand, the principal contributions to excitation 15 are the L2 → Mo $d_{x^2-y^2}$ and L4 → Mo d_{yz} β-electron transitions. Again, the weak excitation 16, due to the mixture of the β-electron transitions represented by L1 → Mo $d_{x^2-y^2}$ and L2 → Mo $d_{x^2-y^2}$ is included as well. Note that the L1 and L2 orbitals resemble the $b_1(\sigma)$ and $a_2(\pi)$ combinations from the simple thiolate fragment (Figure 6). Additionally, one point that might be important to keep in mind is that although the dithiolate groups contribute significantly to the ligand-based orbitals involved in the transitions, there

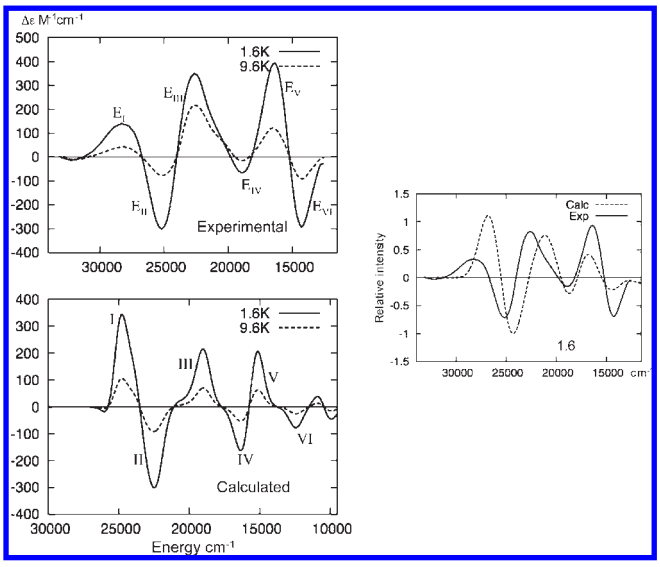

Figure 9. Experimental[25] (top left) and simulated (bottom left) MCD spectra at different temperatures, 1.6 and 9.6 K and 4.5 T. For the creation of the figure to the right, the calculated spectra at 1.6 K blue-shifted by 2000 cm^{-1} (0.25 eV). The experimental bands are labeled E_I to E_{VI}, and the calculated bands are marked by the roman numerals I to VI.

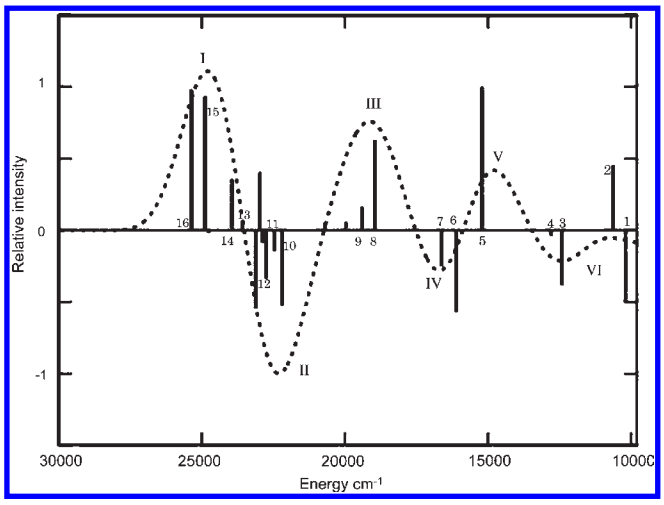

Figure 10. Normalized simulated MCD spectrum. The bars indicate the relative intensity of the C_J-parameter for each calculated excitation.

is also some evident participation of p-orbitals from the OCH_3 and OH ligands.

The MCD spectrum of the Mo[V]-DMSOR enzyme has been recorded by Thomson et al.[25] and Johnson et al.[26] The experimental spectra[26] recorded with a magnetic field of 4.5 T at 1.6 and 9.6 K are shown in Figure 9. The spectra consist of three positive peaks at 28750 (E_I), 22900 (E_{III}), and 16000 cm^{-1} (E_V); and three negative peaks at 25400 (E_{II}), 19000 (E_{IV}), and 14750 cm^{-1} (E_{VI}). Additionally, a weak negative MCD band was observed around 11000 cm^{-1}, although the data was not shown.[26]

From a simple model based on a Mo(V)-dithiolene fragment with C_{2v} symmetry (Figure 6), the two bands with opposite sign, E_V and E_{VI}, were assigned to the $a_2(\pi) \rightarrow$ Mo d_{yz} and $2b_2(\pi) \rightarrow$ Mo d_{yz} transitions (where Mo d_{yz} represents the HSOMO), respectively.[25,26] The $a_2(\pi)$, $1b_2(\pi)$, $2b_2(\pi)$, and $b_1(\sigma)$ linear combination of p orbitals from the thiolene fragment are shown in Figure 6. Thomson et al. assigned the band E_{III} to the transition $1b_2(\pi) \rightarrow$ Mo d_{yz}, while Johnson et al. assigned it to a $2b_2(\pi) \rightarrow$ Mo d_{xz} (LUMO) transition and the E_{IV} band was assigned to the $1b_2(\pi) \rightarrow$ Mo d_{yz} transition. The bands at higher energies were tentatively suggested to arise from dithiolene sulfur orbitals which form σ-bonds to the metal center or from other ligands such as an oxygen-based group or even histidine ligands.[25] However, Johnson et al. assigned the E_I and E_{II} bands to the $1b_2(\pi) \rightarrow$ Mo d_{xz} and $a_2(\pi) \rightarrow$ Mo d_{xz} transitions, respectively.[26] Further, on the basis of electronic spectral studies of $LMoO(SCH_2CH_2S)$, L = hydrotris(3,5-dimethyl-1-pyrazol)borate, Carducci et al.[45] assigned the bands E_I, E_{II}, and E_{III} of Figure 9 to the presence of two pseudo-A terms. The one at at higher energy was formed by the transitions $S_{\pi b_2} \rightarrow$ Mo d_{xz} and $S_{\pi b_2} \rightarrow$ Mo d_{xy}. The other pseudo A-term was proposed to arise from the transitions $S_{\pi a_2} \rightarrow$ Mo d_{xz} and $S_{\pi a_2} \rightarrow$ Mo d_{xy}. E_{IV} was assigned to the $d_{yz}-d_{z^2}$ transition. Finally, it was suggested that the pseudo-A term (bands E_V and E_{VI}) was due to the transition involving the additional sulfur atoms coordinated to molybdenum in DMSOR and that are not present in $LMoO(SCH_2CH_2S)$.

The simulated MCD spectra, calculated at 1.6 and 9.6K with a magnetic field strength of 4.5 T are displayed in Figure 9. They exhibit, as in the case of the experimental ones, 3 positive MCD-bands with maximum intensities around 25000, 19000, and 15000 cm^{-1} (I, III, and V in Figure 9) and 3 negative bands around 22000, 16400, and 11500 cm^{-1} (II, IV, and VI in Figure 9). Additionally, a weak pseudo A-term appears around 10000 cm^{-1} in accordance to the observations of Johnson et al. It is known that in a TDDFT calculation, the expected error for transitions well-described by one-electron excitations and systems without a transition metal, is about 0.2−0.3 eV.[46] For a better quantitative comparison between the experimental and simulated spectra, a blue-shift of 2000 cm^{-1} (0.25 eV) is applied to the calculated MCD spectra. The superposition of the experimental and calculated spectra at 1.6 K can be found in Figure 9. It includes both an energy shift and a broadening of the band shape function.

Figure 10 displays the simulated normalized MCD spectrum (without the shifting but with the broadening of the signals) with the individual C-parameters indicated as bars. Table 4 contains the relevant C_J parameters and their contributions from the C_J^G and C_J^E terms. Both C_J^E and C_J^G are calculated directly by response theory.[40,47] It follows from Table 4 that in all but two cases (excitations 4 and 9), C_J^E is the dominant contribution. Using the sum-over-states expression of the form given in eq 11 it was further possible to identify the excited states that provide the most significant contributions to each C_J^E term. These states are listed in Table 4. Moreover, the excited state making the largest contributing to C_J^G is also shown in Table 4 for the cases where $C_J^G > C_J^E$.

(45) Carducci, M. D.; Brown, C.; Solomon, E. I.; Enemark, J. H. *J. Am. Chem. Soc.* **1994**, *116*, 11856.

(46) Jacquemin, D.; Perpète, E. A.; Ciofini, I.; Adamo, C. *Theor. Chem. Acc.* **2008**, *120*, 405.

(47) Seth, M.; Krykunov, M.; Ziegler, T.; Autschbach, J. *J. Chem. Phys.* **2008**, *128*, 234102.

Table 4. Principal *C* Parameters[a] from Model **4**′[b]

C-term	J^d	C_J	C_J^G	K'	C_J^E	K^d
I	16	17.15	−0.11		17.26	h
	15	16. 38	−0.94		17.32	g,h[e]
	14	6.24	1.30		4.94	12,10
	13	1.02	−1.02		2.04	14
II	12	−5.87	0.09		−5.96	14
	11	−2.54	0.74		−3.28	12
	10	−9.16	−0.48		−8.68	14
III	9	2.89	3.38	9	−0.49	8
	8	10.98	3.62		7.36	9,10
IV	7	−4.33	0.11		−4.44	5,9
	6	−9.93	0.95		−10.88	5,8
V	5	17.46	0.31		17.15	6,7
VI	4	−0.68	−1.45	4	0.77	3,5
	3	−6.70	−1.78		−4.92	4
	2	7.95	−0.38		8.33	1
	1	−8.78	−1.37		−7.41	2

[a]Values in au × 10^{-3}. [b]C_J is the total value, C_J^G is the contribution due to the spin-orbit coupling perturbation of the ground state. C_J^E is the contribution from the perturbation of the excited state J^c. K′ and K are the excited states with the most significant contribution to the total value of C_J^G and C_J^E. [c]For details, see eq 12. [d]See Table 3 for details on the excitations. [e]Excitation "g" is described in the Supporting Information, and excitations "h" are calculated at high energy, around 26000 cm^{-1}

We shall now elaborate on the origin of the simulated C-terms labeled from I to VI in Figure 10. Our simulated C-term "I" indicates that the positive band around 28000 cm^{-1} contains several excitations, as well as that our assignment for some of them is in line with the previous assignments. There are three intense *C*-parameters corresponding to excitations 14, 15, and 16 that may be considered to be almost completely responsible for the positive MCD-band "I" (Figure 10). As discussed earlier, we assigned excitations 16 and 15 to correspond to a ligand (L1, excitation 16 or L2, excitation 15) → $d_{x^2-y^2}$ transition, while the L3 → d_{xz} transition corresponds to excitation 14. The L1 orbital can be compared with the $b_1(\sigma)$ combination in Figure 6, L2 with $a_2(\pi)$, and L3 with $2b_2(\pi)$. So, excitation 14 contains some of the same assignments proposed by Johnson,[26] Carducci,[45] and co-workers. Previously, Thomson et al. hypothesized that CT transitions were expected from dithiolene sulfur orbitals able to form σ-bonds such as the $b_1(\sigma)$ combination.[25] The dominant contributions to the parameters C_{15} and C_{16} are due to the perturbation of the respective excitation with excitations g and h (Table 4). On the other hand, the value of the C_{14}-parameter is dominated by the spin−orbit coupling of excitation 14 with excitations 12 and 10.

Figure 10 shows that the adjacent negative MCD-band "II" is mostly due to *C*-parameters at 22760 (excitation 12) and 22200 cm^{-1} (excitation 10). We assigned the former to a d_{yz} → d_{z^2} transition (such an assignment had not been done in the previous studies) and the latter to a $2b_2(\pi)$ (L3) → $d_{x^2-y^2}$. The main contribution to C_{12} and C_{10} arises from the spin−orbit coupling interaction between excitation 12 (or 10) and excitation 14. Note that Carducci et al. assigned band "II" to the transitions $S_{\pi b_2}$ → Mo d_{xy} and $S_{\pi a_2}$ → Mo d_{xz}.[45] The latter assignment for this band was also made on the basis of the simple fragment in Figure 6.[26] We calculated one excitation with a similar assignment contained within the simulated MCD-band "II". Excitation 11 is due to the $a_2(\pi)$ (L2) → $d_{x^2-y^2}$ transition (Table 3), but we need to recall that the orbital we named Mo $d_{x^2-y^2}$ has in fact a considerable contribution from the atomic orbital d_{xz} (Figure 4). Moreover, the inspection of band "II" in Figure 10 shows the presence of a pseudo-A parameter. However, because of the bandwidth of the signals, the overall C-term is negative. A description of those bands, and the rest of the other bands that are not being discussed here, is included as Supporting Information.

Next, the positive C-term "III" was calculated to be mostly due to two *C*-parameters at 18950 and 19410 cm^{-1} corresponding to excitations 8 and 9, respectively. Both excitations consist of transitions from L3 to Mo $d_{x^2-y^2}$ (excitation 8) or Mo d_{xz} (excitation 9). From Table 4, we see that C_9 is dominated by the term arising from the perturbation of the ground state. Further, it was possible to identify that the coupling between the ground state and the excitation 9 represents the major contribution to the C_J^G term. On the other hand, the C_8 is dominated by the C_J^E term due mainly to the spin−orbit coupling with excitations 9 and 10. If we consider the orbital L3 as the equivalent of the $2b_2(\pi)$ linear combination, in this instance, our assignment and the one by Johnson et al. is the same. Moving on to the next band, Carducci et al. assigned the negative C-term "IV" to a d-d transition.[45] However, our calculations indicate that the excitations giving rise to the MCD-term are dominated by two ligand to metal transitions giving rise to the negative *C*-parameters, at 16120 (excitation 6) and 16630 cm^{-1} (excitation 7). Those excitations involve transitions from a $2b_2(\pi)$ combination (L3 or L4) to the Mo d_{xz} or Mo d_{yz} orbitals, respectively. In contrast, according to the simple ligand orbital diagram of Figure 6, "IV" was assigned by Johnson et al. to the $1b_2(\pi)$ → Mo d_{yz} transition.[26] With respect to the origin of the *C*-parameters, Table 4 shows that the negative C_6 is mainly due to the spin−orbit coupling perturbation of excitation 6 mixing with excitations 5 and 8, while the C_7 arises from the mixing of excitation 7 with 5 and 9. The positive MCD-band "V" comes from excitation 5. Here, excitation 5 mixes with 6 and 7. We should recall that the parameters C_6 and C_7 have a predominant contribution from the spin orbit coupling with excitation 5. We will come back to this point later in this discussion. Excitation 5 is mainly composed of a transition from the L4 ($2b_2(\pi)$) to the Mo $d_{x^2-y^2}$ orbitals (Table 3). Johnson et al. and Thomson et al. assigned this to a $1a_2(\pi)$ → Mo d_{xz} transition.[25,26] Finally, because of the broadening of the signals, the last negative weak band "VI" arises from four *C*-parameters. The one at 12800 cm^{-1} (C_4) comes from a L4 ($2b_2(\pi)$) → Mo d_{xz} transition (excitation 4) mixing mainly with excitations 3 and 5, and the parameter C_3 at 12420 cm^{-1} appears from a L4 → Mo $d_{x^2-y^2}$ transition. This parameter is mainly due to the spin−orbit coupling perturbation of excitation 3 by excitation 4. Thomson et al. and Johnson et al. assigned this band to the $a_2(\pi)$ → Mo d_{xz} transition.[25,26] The last two C-parameters to be discussed, C_1 and C_2 form a pseudo-A term structure (Figure 10). Both parameters arise from d-d transitions (Table 3), and their values are mainly due to the spin−orbit perturbation of both excitations coupling with each other.

In general, the MCD spectrum shown in Figure 9 is dominated by C_J^E contributions and has the appearance

of C-terms with alternating signs (pseudo-A terms). We can understand this pattern by observing from eq 14, that for a contribution to C_J^E from excited state K, there will be a contribution to C_K^E from excited state J of the opposite sign, as follows

$$C_J^E = \sum_{\alpha\beta\gamma} \varepsilon_{\alpha\beta\gamma} \langle A|M^\alpha|K\rangle^{(0)} \langle J|M^\beta|A\rangle^{(0)} \frac{\langle J|H_{SO}^\gamma|K\rangle^{(0)}}{E_K - E_J}$$

$$= \sum_{\alpha\beta\gamma} \varepsilon_{\beta\alpha\gamma} \langle A|M^\beta|K\rangle^{(0)} \langle J|M^\alpha|A\rangle^{(0)} \frac{\langle K|H_{SO}^\gamma|J\rangle^{(0)}}{E_J - E_K}$$

$$= -C_K^E \quad (16)$$

since $\varepsilon_{\alpha\beta\gamma} = -\varepsilon_{\beta\alpha\gamma}$. This becomes important when the J and K states are adjacent, and their mixing via spin−orbit coupling constitute the main contribution to the total value of the corresponding C-parameter as discussed, for example, in the case of the C_1 to C_4 parameters.

It has been pointed out elsewhere[48] that one issue arising from the sum-over-states formulation of eq 16 is that the strong influence of the energy denominator puts very heavy demands on the theoretical method used to calculate the transition energies. This is certainly true in our case, because the shape of a resulting pseudo-A term structure might be independent of the relative order of the two involved states.[49] However, the situation is different for pseudo-A terms due to states with an energy difference larger than their absorption bandwidths. In this case, assignments of the excitations that give rise to the corresponding C-terms should be unambiguous if the calculated MCD spectrum reproduces the right form when compared with the experimental spectrum. Now, for close lying excited states it may not be possible to provide an unambiguous assignment of the electronic transitions within the framework of TD-DFT. But if the energy difference between those states is signicantly smaller than their absorption bandwidths, the C-parameters may appear as only one band, and it is still possible to describe the nature of the transitions that make up the MCD-band. Obviously, the energy order of the participating close-lying states still remains uncertain.

Finally, a comparison of eqs 11 and 15 indicates that there is a relation between Δg_{st} and C_J^G in that both depend on the mixing of the ground state with excited states due to the spin−orbit coupling. One might thus have thought that the same excited states K' would be important for C_J and Δg_{st}. This is not the case since C_J is dominated by C_J^E rather than C_J^G. Further, Δg_{st} has the largest contributions from d-d transitions and these transitions are not relevant for C_J^G in the cases where it contributes significantly to C_J. Thus, for the system at hand, the EPR and MCD spectroscopy do not reflect much on each other with respect to their physical origin.

(48) Seth, M.; Autschbach, J.; Ziegler, T. *J. Chem. Theory Comput.* **2007**, *3*, 434.
(49) Neese, F.; Solomon, E. *Inorg. Chem.* **1999**, *38*, 1847.

Concluding Remarks

We have discussed the calculated EPR parameters for 4 different models of Mo[V]-DMSOR constructed from one available X-ray structure of the oxidized Mo[VI] DMSOR enzyme.[5] We see that the most stable structure, model **2**, yields EPR parameters within reasonable agreement with the experimental values, except for the g_1 component of the g-tensor. In this model, the $H_{OH}-O_{OCH3}$ distance was allowed to be optimized. However, when this distance is constrained to a value of 2.8 Å as proposed by Raitsimring et al.[9] the agreement with the experimental EPR parameters is improved, as in the case of model **3**. However, one problem with model **3**, where the position of the nitrogen from the pyrrole group was kept frozen, is that the ^{1}H HFC gives rise to a small value compared to experiment. However, once the position of the pyrrole group is allowed to be optimized while keeping the O−H distance constraint, as in model **4**, a very reasonable agreement, both with the g-values and the proton hyperfine coupling constant, is obtained. Thus, model **4** with a $H_{OH}-O_{OCH3}$ constraint at 2.8 Å as proposed by Raitsimring et al.[9] affords the best fit between observed and calculated EPR parameters. From the results of the calculations it is seen that the g-tensor is very sensitive to the orientation of the hydroxide ligand, while the ^{1}H HFC is, not surprisingly, mostly affected by the surrounding groups interacting with the proton of the hydroxide ligand. Unfortunately, a direct determination of the Mo[V]-DMSOR structure would require the inclusion of the protein matrix and this is not yet computationally feasible.

Our simulation of the MCD spectrum for Mo[V]-DMSOR is based on a simple model that only takes into account the immediate ligands coordinated to the molybdenum center. We obtained a simulated spectrum in good agreement with experiment after a blue-shift by 0.25 eV of all the calculated parameters. It was found that the C-parameters in the MCD spectrum are dominated by mixing of excited states (C_J^E) because of spin−orbit coupling rather than mixing of excited states with the ground state (C_J^G). In this case, the appearance of C-terms in the MCD spectrum of alternating signs was related to the fact that a contribution to C_J^E from excited state K will be followed by a contribution from excited state J to C_K^E of opposite sign as shown in eq 16. We have finally compared our assignments of the different MCD and absorption bands to those given by Thomson et al.,[25] Johnson et al.,[26] and Carducci et al.[45] The previous studies, usually assigned a single excitation to a given MCD-band, and our simulation indicates that, most of the times for our systems, each MCD signal contains several excitations.

Acknowledgment. All calculations were performed using the Western Canada Research Grid computing resources (www.westgrid.ca). This work was supported by NSERC. T.Z. thanks the Canadian government for a Canada Research Chair.

Supporting Information Available: The orbitals HOMO-10 to HOMO+9 are presented. Note that HOMO-4 to HOMO+4 have been discussed. The description of the remaining transitions that make up the calculated absorption spectrum is also presented there. This material is available free of charge via the Internet at http://pubs.acs.org.